Eur. Phys. J. D **33**, 301–306 (2005)
DOI: 10.1140/epjd/e2005-00042-8

THE EUROPEAN PHYSICAL JOURNAL D

Nonlinear Thomson scattering from relativistic laser plasma interaction

K. Ta Phuoc[a], F. Burgy, J.-P. Rousseau, and A. Rousse

Laboratoire d'Optique Appliquée, ENSTA, CNRS UMR 7639, École Polytechnique, Chemin de la Hunière, 91761 Palaiseau, France

Received 6 September 2004 / Received in final form 8 December 2004
Published online 12 April 2005 –

Abstract. As an electron oscillates in an intense laser field, it acquires a highly nonlinear motion and emits X-ray radiation by nonlinear Thomson scattering. In this paper we present a numerical and experimental analysis of this radiation. We show that this radiative process becomes dominant at relativistic laser intensities ($a_0 > 1$), for which the laser light scatters off MeV electrons accelerated in the plasma.

PACS. 52.38.Ph X-ray, gamma-ray and particle generation – 52.25.Os Emission, absorption, and scattering of electromagnetic radiation – 52.50.Dg Plasma sources

1 Introduction

Since lasers can provide intensities greater than 10^{18} W/cm^2, laser-plasma interaction can be studied in the relativistic regime and highly nonlinear physical mechanisms are brought to light [1]. Important features of the laser energy absorption and plasma dynamics have been revealed like the acceleration of electrons to relativistic energies from the space charge separation fields within the plasma. However, only a few studies have been concentrated on the radiative properties associated with the strongly nonlinear motion of the plasma electrons as they oscillate in the laser field [2–11]. We show in this paper that nonlinear Thomson scattering can be a significant radiative mechanism during the interaction. As a result, an anisotropic and polychromatic radiation can be produced with a spectrum peaked in the X-ray energy region extending up to the kilo-electronvolt (keV) range with the intense laser systems currently available [10]. In this paper we present a spectral and angular characterization of this radiative mechanism as well as the dependencies with the laser and plasma parameters. The paper is organized as follow: using a test particle simulation we first give a simple numerical description of the properties of nonlinear Thomson scattering radiation emitted by an electron oscillating in an intense laser field. We then describe and discuss the experimental results obtained during the interaction of a 50 TW (30 fs) laser pulse with a helium plasma.

[a] e-mail: kim.taphuoc@ensta.fr

2 Electron motion in an intense laser field

In our simulations, we consider a laser field approximated by a plane electromagnetic wave. It propagates in the x-direction, has a frequency ω_0, and is linearly polarized along the y-direction. The temporal envelope of the laser pulse, in amplitude, is assumed to follow a $\sin^2$ function. The intensity I is expressed as a function of the normalized vector potential

$$a_0 = 0.85\sqrt{I_{[10^{18}\ \mathrm{W/cm^2}]}\lambda^2_{0[\mu\mathrm{m}]}}$$

where $\lambda_0 = 2\pi c/\omega_0$ with c the speed of light. The equation of motion of the electron submitted to the laser field is given by

$$\frac{d\mathbf{p}}{dt} = e\mathbf{E} + \frac{\mathbf{v}}{c} \wedge \mathbf{B}$$

where e and m are the charge and mass of the electron, $\mathbf{E}$ and $\mathbf{B}$ are the electric and magnetic fields of the laser. We consider that the electron is free (the restoring force due to the space charge separation between the electron and the ions background in the plasma, weak for intense femtosecond laser pulse and low density plasma, has been neglected). When the electron is initially at rest, the equation of motion can be solved analytically by using the transverse symmetry and the invariance of the Lagrange function [12]. In that case, the transverse and longitudinal components of the electron momentum $\mathbf{p}$ (normalized to mc) are directly related to the normalized vector potential $\mathbf{a} = (\mathbf{A}/mc^2)$ of the laser field as $p_\perp = a_\perp$, $p_\parallel = ea^2/2$ where $a_\perp$ is the transverse component of $\mathbf{a}$. For arbitraries

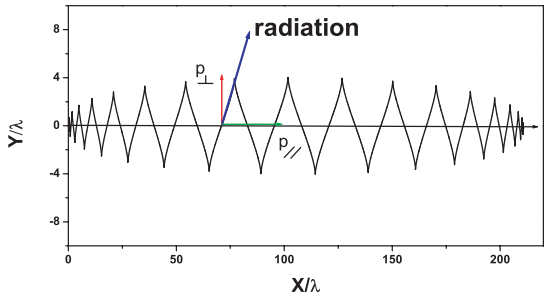

Fig. 1. Electron trajectory. The electron is initially at rest, the laser parameters are $a_0 = 5$, $\tau = 30$ fs.

initial conditions, the equation of motion is integrated numerically using a Runge-Kutta method. The well-known trajectory of an electron in such intense laser field is displayed in Figure 1 for the case of a 30 femtosecond laser pulse and $a_0 = 5$. We can observe that the electron experiences a forward drift motion in the direction of the laser propagation and undergoes transverse oscillations in the plane of the laser polarization. As a consequence of the a^2 dependence of the longitudinal momentum, the trajectory is mainly transverse for $a_0 \ll 1$ and mainly longitudinal for $a_0 > 1$.

3 Nonlinear Thomson scattering

Thomson scattering radiation is produced as the electron oscillates in the laser field. In the linear case, for $a_0 < 1$, the electron has a linear oscillating motion and radiates at the fundamental frequency (the laser frequency). Here we discuss the nonlinear case, where the motion of the electron, driven by a high intensity laser field ($a_0 > 1$), becomes strongly nonlinear and relativistic. The electron then radiates high orders harmonics, often called relativistic harmonics [5–7]. By using the trajectories calculated above, the radiation emitted by the electron can be obtained from the formulae of the radiation emitted by an accelerated charged particle [13]. The spectral flux emitted by a single electron in the direction $\mathbf{n}$ is given by:

$$\frac{d^2I}{d\omega d\theta} = \frac{e^2}{4\pi^2 c}\left|\int_{-\infty}^{+\infty} e^{i\omega(t-\mathbf{n}\cdot\mathbf{r}(t)/c)}\frac{\mathbf{n}\times\left[(\mathbf{n}-\beta)\times\dot{\beta}\right]}{(1-\beta\cdot\mathbf{n})^2}dt\right|^2.$$

It depends on the direction of observation $\mathbf{n}$, the position $\mathbf{r}(t)$, the normalized velocity $\beta(t)$ and the acceleration $\dot{\beta}(t)$ of the electron. The radiation is therefore anisotropic and strongly linked to the laser parameters.

The angular distribution of the total power radiated by the electron, integrated over all frequencies, is displayed in Figure 2. The radiation is emitted forward along two lobes centered on the directions of maximum momentum of the electron, corresponding to the angles $(\theta_{max}, -\theta_{max}) \sim \tan^{-1}(p_\perp/p_\parallel)$. The divergence angle of each lobe is therefore given by $\theta_{max} \sim 2/a_0$ and is directly related to the laser intensity. As shown in Figure 2A

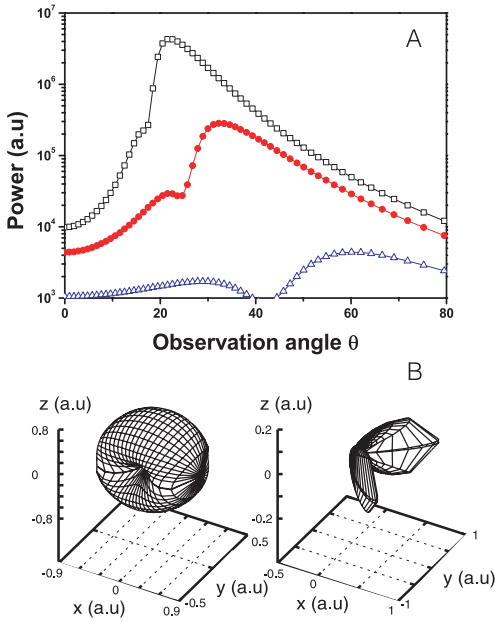

Fig. 2. (A) Angular distribution of total power of the radiation for $a_0 = 2$ (triangles), 4 (circles) and 6 (squares) in the plane of polarization. The laser is linearly polarized. $\theta = 0°$ corresponds to the laser axis. (B) 3D representation of the spatial distribution for $a_0 = 0.1$ and $a_0 = 3$.

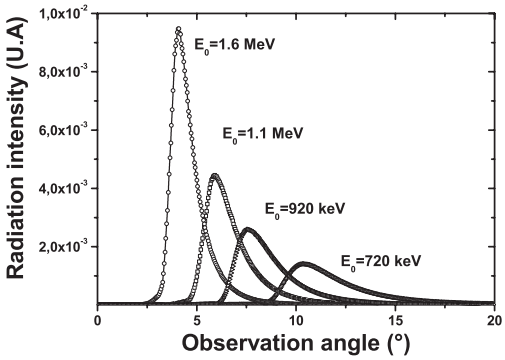

Fig. 3. Influence of the initial energy of the electron on the angular distribution of the radiation.

the spatial distribution of the radiation is broad and becomes more collimated as a_0 increases. For $a_0 = 4$ and $a_0 = 6$ the divergences are respectively $\theta = 34°$ and $\theta = 20°$. In Figure 2B we have represented the spatial distribution for $a_0 = 0.1$ and $a_0 = 2$. For $a_0 = 0.1$ (nonrelativistic case) a typical dipolar emission is observed while two lobes of emission are already seen for $a_0 = 2$. If we now consider that the electron has an initial longitudinal energy, the angular distribution of the radiation is then strongly modified. The component $p_\parallel$ of the momentum is increased, which directly results in a more collimated radiation. Figure 3 displays the numerical simulations taking into account this effect on the angular distribution of the radiation. It shows that electrons with an initial energy of 0.7 MeV produce an emission centered at $\theta = 10°$ instead of being centered at 23° for the case of an electron

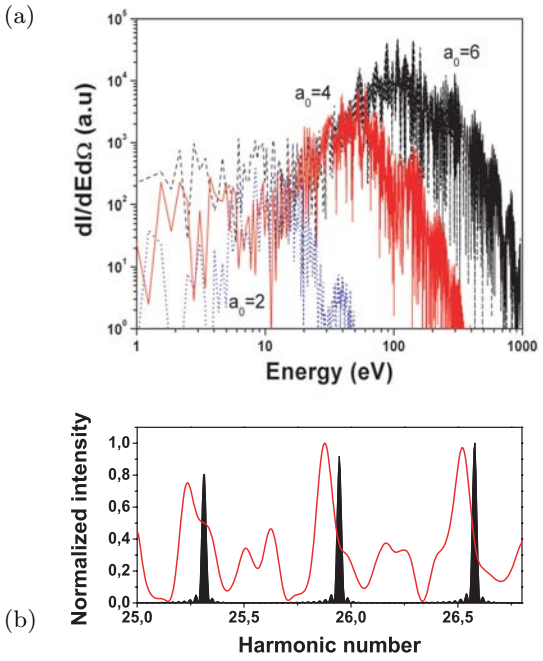

Fig. 4. (a) Spectrum of the nonlinear Thomson scattering radiation estimated at the angle of maximum emission for $a_0 = 2$ (doted), 4 (solid) and 6 (dashed). (b) Detailed structure of the spectrum calculated for $a_0 = 6$ for an infinite plane wave and for a 30 fs laser pulse. In each case, the radiation is calculated at the angle of maximum power. The spectrum consists on discrete harmonics for an infinite plane wave and becomes a continuum for a short laser pulse.

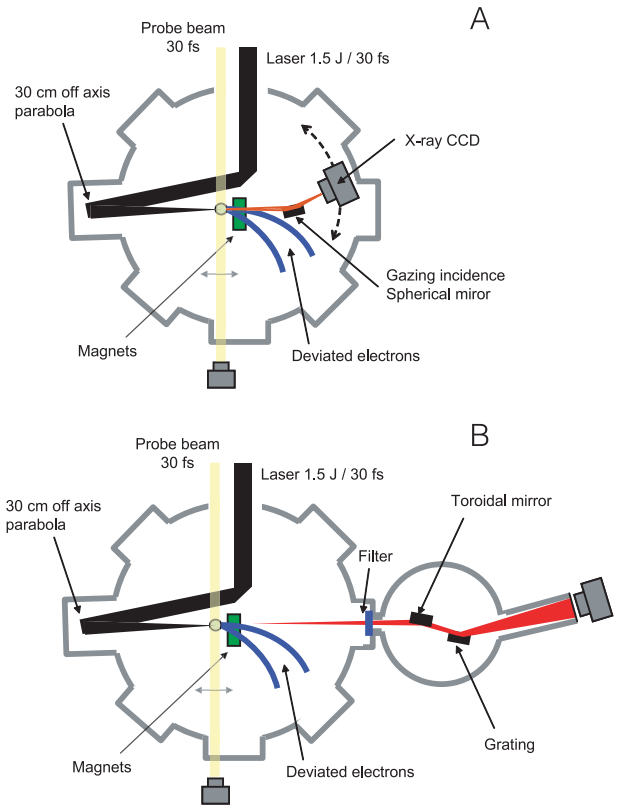

Fig. 5. Experimental set-up. The laser is focussed using a 30 cm off axis parabola onto the front edge of a supersonic helium gas jet. (A) The X-ray CCD is mounted on a rotation stage centered on the gas jet. Filters (Al, Zr, Ti) are placed in front of the CCD to block the laser light. A spherical mirror is used at grazing incidence to collect and focus the X-ray radiation onto the detector. (B) The X-ray signal is analyzed using an imaging spectrometer composed of a toroidal mirror at grazing incidence, a reflection grating and a back illuminated X-ray CCD. Filters are placed at the entrance of the spectrometer.

initially at rest. Electrons at 1.6 MeV further collimate the radiation to 4°.

The spectrum of the radiation, calculated at angles of maximum emission θ_{max}, is displayed in Figure 4a for $a_0 = 2$, 4 and 6. The spectrum is broad, peaked, quasi-continuous and exhibits complex structures. It extends from eV to a few hundreds eV. The position of the peak shifts to higher energies as a_0 increases. For $a_0 = 2$, 4 and 6 the peaks are respectively found at 10 eV, 60 eV, 100 eV. Simulations performed as a function of the observation angle have also shown that the most energetic radiation is produced at the angle of maximum power θ_{max}. For other angles, the spectrum shifts to smaller energies. Finally, the shape of the spectrum significantly depends on the laser pulse duration. As shown in Figure 4b for an infinite plane wave, the spectrum consists on well separated harmonics which are not at integral number of the laser wavelength. Their spectral separation depend on the observation angle, the laser intensity, and the initial energy of the electron. In the case of short laser pulses, the electron motion becomes strongly modulated in the laser pulse envelope and the consecutive harmonics overlap to form a continuous spectrum. Compared to the case of the infinite plane wave, we observe a shift in the harmonic structure of the spectrum for the short pulse. This may be explained by the fact that electrons experience $a_0 = 6$ only at the peak of the pulse. The radiation contribution from electrons experiencing to lower values of a_0 within the pulse, is significant and located at smaller energies.

4 Experimental set-up

The experiment has been conducted at the Laboratoire d'Optique Appliquée (LOA) where we used a 30 fs and 1.5 J (50 TW) Ti:Sa laser system [13]. The contrast of the laser pulse is 10^{-7} in intensity. The experimental set-up is shown in Figure 5. The laser beam, 55 mm in diameter, was focused with an $f/5.45$ off-axis parabolic mirror onto the front edge of a supersonic cylindrical gas jet of helium (3 mm in diameter) [15]. Electronic densities from 10^{18} cm^{-3} to few 10^{19} cm^{-3} were used in the experiment. The diameter of the focal spot was 6 μm at full width half maximum (FWHM) in intensity and contained 60% of the laser energy. The maximum incident laser intensity (I) was 7×10^{19} W/cm^2, which corresponds to a laser strength parameter $a_0 = 5.6$ for linear polarization.

The X-ray radiation was first analyzed using an X-ray CCD placed in the interaction chamber. The angular dependency of the X-ray emission was obtained by rotating the X-ray CCD around the laser focal spot. For this measurement, a filter (aluminium, zirconium or titanium) was placed in front of the detector and provides large spectral bandwidth selection. A static and 0.5 Tesla magnetic field was inserted after the plasma to deviate the electrons accelerated in the forward direction out of the detector. To measure accurately the spectrum of the radiation, we then used an XUV spectrometer composed of a toroidal mirror at grazing incidence (4 degrees), a gold coated reflection grating (600 lines/millimeter) and a back illuminated X-ray CCD. At the entrance of the spectrometer, aluminium, zirconium and titanium filters with thicknesses between 150 nm to 300 nm were positioned to block the laser infrared light. The response of the spectrometer was determined by considering the filters transmission, the mirror reflectivity, the grating efficiency and the detector response.

Finally, a second arm of the laser system was used to optically probe the propagation of the beam inside the cylindrical gas jet by shadowgraphy imaging. Electrons accelerated in the forward direction inside the plasma were characterized using radio-chromic films and a set of filters in the 100 keV and MeV range as well as a magnetic spectrometer positioned in the forward direction [16] in the 10 MeVs range.

5 Experimental results

We have characterized the angular distribution, the spectrum and the dependencies of the X-ray radiation produced during the interaction as a function of the laser and plasma parameters. In this section we demonstrate that the features of the observed X-ray signal are consistent with the expected unique properties of the nonlinear Thomson scattering: the spatial distribution of the radiation is anisotropic, the spectrum is broad, continuous and peaked, and the X-ray intensity grows linearly with the electron density. However, we show that the laser-plasma interaction involves more complex physical mechanisms than the model of an electron initially at rest. In the experiment, electrons are accelerated in the forward direction and have a net energy gain. As they oscillate in the laser field, these electrons have an additional energy that must be taken into account for the calculation of the nonlinear Thomson scattering radiation.

The angular distribution of the X-ray radiation, integrated between 70 and 200 eV and measured in the plane of the laser polarization, is displayed in Figure 6. It is found to be much broader than the theoretical width (10°) expected if the electron is considered to be initially at rest. It is also centered on the laser axis ($\theta = 0$) instead of 23° for $a_0 = 5.6$. Similar results were obtained at all the X-ray spectral bandwidths. However, as we already discussed, the properties of the radiation produced depend on the electrons parameters [17]. The angular distribution is significantly modified, broadened, and shifted toward

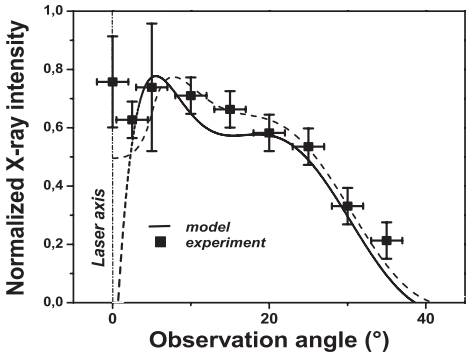

Fig. 6. Spatial distribution of the observed X-ray emission integrated over the spectral bandwidth of the zirconium filter (∼70–200 eV) for $a_0 = 5.6$. For this measurement, the X-ray CCD was placed in the interaction chamber and rotated around the gas jet. A zirconium filter was placed in front of the CCD. The solid line (dotted line) is the numerical result obtained for an electron distribution with a temperature of 0.9 MeV and without (with) 5° **k** spread.

the laser axis if the electrons experience an acceleration coming in addition to the laser field. This is the case in this experiment, where electrons accelerated in the forward direction have been clearly measured with radiochromic films covered by copper filters. Although the set of filters did not allow the characterization of the distribution function, the measurements indicate a strong population of electrons with energies between a few hundreds keV and a few MeV.

This population of electrons, which was also seen using a PIC simulation, can either come from the plasma wave acceleration or from a phase mismatch of the electrons inside the laser field due to collisions in the plasma. In addition, the PIC simulation shows that this population of accelerated electrons (which have energies in the few hundreds keV to a MeV range) exists within the laser pulse and feel its electromagnetic field. They can therefore be considered as electrons having an initial energy as they oscillate in the laser field. An electron distribution function, as seen in this experiment, can then clearly broaden the X-ray signal and center it towards the axis. Notice that in this parameter regime, more energetic electrons (above a few MeV) are observed. These electrons are actually accelerated in the wake of the laser pulse and do not oscillate in the laser field.

The best fit of the experimental data is represented by the solid line in Figure 6 by also taking into account the contribution of a 5° spread which can either originate from the divergence of the electron beam or from the spread of the **k**-vectors of the focused laser. An electron distribution function $\exp(-E/E_0)$ characterized by an electronic temperature of 0.9 MeV ± 0.3 MeV is retrieved. The choice of the temperature is fully driven by the angular distribution of the radiation observed. This temperature is consistent with the electrons energies measured in the experiment and observed in the PIC simulation. If higher temperatures are considered, the radiation becomes more collimated and can not reproduce the width

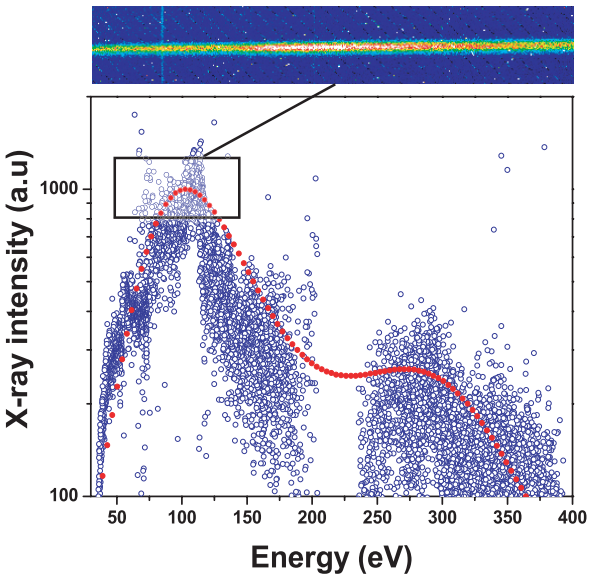

Fig. 7. Experimental spectrum obtained on axis for $a_0 = 5.6$. Aluminium, zirconium and titanium filters were placed at the entrance of the spectrometer to block the laser light. The CCD image obtained at the peak of the spectrum is presented. The fit is obtained from the numerical simulation for $a_0 = 6$, $\gamma_0 = 3$ and at $\theta = 3°$.

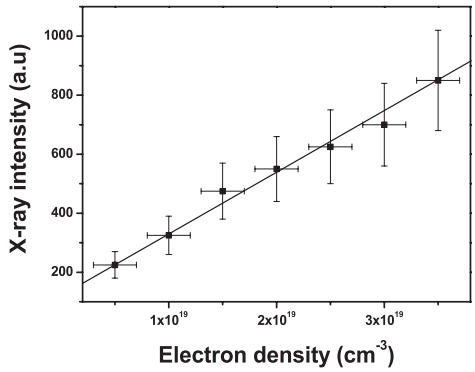

Fig. 8. X-ray intensity as a function of the electron density of the plasma at an X-ray energy of 100 eV.

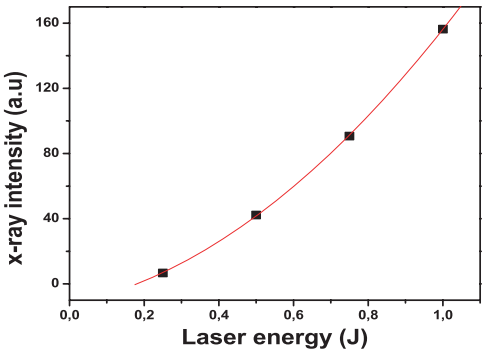

Fig. 9. X-ray signal as a function of the laser energy.

of the distribution; for weaker temperatures, the distribution shifts off axis.

The spectrum of the radiation measured on the laser axis, at the maximum X-ray intensity and for $a_0 = 5.6$, is displayed in Figure 7. Efficiencies of all the components of the spectrometer are taken into account. A broad continuum extending from 20 eV to 400 eV is observed (the spectrometer did not allow a characterization below 20 eV and above 400 eV). It is peaked at 100 eV which is in close agreement with the numerical simulation done for $a_0 = 6$ and an electron with $\gamma = 3$ as shown in Figure 7. The X-ray intensity then rapidly drops. The spectrum of the radiation also depends on the initial electron energy. However, in this co-propagative geometry this effect is weak because the Doppler shift of the laser frequency seen by the electron is counterbalanced by the Doppler shift on the emitted radiation.

The X-ray intensity measured at the peak of the spectrum (100 eV) as a function of the plasma electron density is displayed in Figure 8. As expected for nonlinear Thomson scattering which is an incoherent radiative process from electrons, the observed X-ray signal is found to increase linearly with the electron density.

Finally, the X-ray intensity was measured as a function of the laser energy as presented in Figure 9. We found a nearly linear growth of the X-ray intensity for the peak of the spectrum.

All of these features exclude that other radiative processes could be at the main origin of the produced X-ray radiation, even if they may participate to the overall emission. First, the radiation is collimated in the forward direction. Collisionnal processes like non-relativistic Bremsstrahlung radiation or radiative recombination have an isotropic angular distribution. Second, the radiation spectrum is continuous and peaked at 100 eV. High harmonics generated from atomic ensemble provide different features. They have a decreasing spectrum with a plateau which consists on well define harmonics [18]. In addition, similar X-ray signal was observed in circular polarization for which this particular radiative mechanism can not exist. Collisionnal processes have a spectrum extending to high energies and can not provide any peak. The signal was found to increase linearly with the electron density whereas collisionnal processes would have scaled as the square of the atomic number. Spatial and time-dependent simulations confirm that the emission from collisionnal processes is still growing with n_e^2. It can not explain the linear dependency on-axis observed here. Finally, relativistic bremsstrahlung which would have a collimated angular distribution is found to be orders of magnitude smaller than the observed X-ray flux.

6 Conclusion

We have demonstrated that the observed X-ray signal follows the unique features of nonlinear Thomson scattering radiation. The radiation is collimated on axis,

the spectrum is a continuum peaked at 100 eV and the X-ray flux grows linearly with the electron density. The simple picture of the free electron oscillating inside the laser field is not sufficient to describe the electron-photon interaction. Additional effects like plasma-accelerated electrons must be taken into account and mostly result in a shift and a broadening of the characteristic angle of emission. We have estimated the number of X-ray photons, integrated over the angular distribution and the spectrum, to be 5×10^{10} per shot. The measurement of the X-ray pulse duration would be an additional confirmation that the X-ray emission is produced by non-linear Thomson scattering.

This work was supported by the European Community under contracts HPRI-CT-1999-00086, HPRI-CT-2000-40016 and HPRI-CT-1999-50004 (FAMTO project). We thank D. Umstadter from CUOS, P. Audebert and J.P. Geindre from LULI and V. Malka from LOA for fruitful discussions.

References

1. D. Umstadter, J. Phys. D: Appl. Phys. **36**, R151 (2003)
2. E.S. Sarachik, G.T. Shappert, Phys. Rev. D **1**, 2738 (1970)
3. E. Esarey, S.K. Ride, P. Sprangle, Phys. Rev. E **48**, 3003 (1993)
4. S.K. Ride et al., Phys. Rev. E **52**, 5425 (1995)
5. S.Y. Chen, M.A.D. Umstadter, Nature **396**, 653 (1998)
6. S. Banerjee et al., Phys. Plasm. **9**(5), 2393 (2002)
7. K. Ta Phuoc et al., Phys. Rev. Lett. **91**, 195001 (2003)
8. K. Lee et al., Phys. Rev. E **67**, 026502 (2003)
9. K. Lee et al., Opt. Expr. **11**, 309 (2003)
10. Y. Ueshima et al., Laser Part. Beams **17**, 45 (1999)
11. Y.Y. Lau et al., Phys. Plasmas **10**, 2155 (2003)
12. J. Meyer-ter-vehn, A. Pukhov, *Atoms, Solids and Plasmas in Super-Intense Laser Fields* (Plenum Publishers, New York, 2001)
13. J.D. Jackson, *Classical Electrodynamics*, 3nd end. (John Wiley and Sons, Inc, New York, 1998)
14. M. Pittman et al., Appl. Phys. B: Las. Opt. **74**, 529 (2002)
15. V. Malka et al., Rev. Sci. Instrum. **71**, 23 (2000)
16. V. Malka et al., Phys. Plasmas **8**, 2605 (2001)
17. P. Tomassini et al., Phys. Plasmas **10**, 917 (2003)
18. T. Brabec, F. Krausz, Rev. Mod. Phys. **72**, 545 (2000)